Dynamical scaling laws in polymers near the glass transition

1991 J. Phys.: Condens. Matter 3 5023

(http://iopscience.iop.org/0953-8984/3/26/021)

J. Phys.: Condens. Matter 3 (1991) 5023–5045. Printed in the UK

Dynamical scaling laws in polymers near the glass transition

L Sjögren
Institute of Theoretical Physics, Chalmers University of Technology, S-412 96 Göteborg, Sweden

Received 2 October 1990, in final form 11 March 1991

Abstract. The mode-coupling theory for the dynamics of supercooled liquids predicts a universal behaviour for the relaxation properties of the β-process. This is completely ruled by generic properties of underlying bifurcation singularities in the non-linear equations of motion, which in the simplest case belong to the cuspoid family A_k; $k \geqslant 2$. The theory gives various scaling scenarios involving one or more parameter scaling functions depending on the order k of the relevant singularity. These predictions are compared with dielectric measurements on the polymeric systems polyethylene terephthalate (PET), polyethylene oxybenzoate (PEOB) and polychlorotrifluoroethylene (PCTFE). Both amorphous and semi-crystalline samples are considered, and in all cases we find a quantitative agreement between theory and experimental results in the relevant frequency region.

1. Introduction

Mode-coupling theories of the dynamics of supercooled liquids make very precise predictions about the frequency and temperature dependence of various correlation functions (see Götze 1990a for an extensive review). Many of the predictions have also been verified even quantitatively by neutron (see Richter *et al* 1989 for a recent summary) and light scattering experiments (Pusey and van Megen 1987, 1990, van Megen and Pusey 1991, Götze and Sjögren 1991a). In these experiments one measures directly the normalized intermediate scattering function or density–density correlation function $\phi_q(t) = F_q(t)/S_q$, as a function of wavevector q and time t or the corresponding Fourier transform $\phi_q''(\omega)$. Here S_q denotes the static structure factor.

The density correlation function can be rewritten in terms of a generalized longitudinal viscosity $M_q(z)$ as

$$\phi_q(z) = -1/\left[z - \Omega_q^2/\left[z + M_q(z)\right]\right] . \tag{1a}$$

Here enters the well known characteristic frequency of the liquid dynamics: $\Omega_q = (q^2v^2/S_q)^{1/2}$, where v denotes the thermal velocity. The viscosity M can be decomposed into two parts: $M_q(z) = \Omega_q^2[m_q^0(z) + m_q(z)]$, where $m_q^0(z)$ describes the details of the liquid dynamics on microscopic time scales. It deals essentially with uncorrelated binary collision events. The most important part of the theory is $m_q(z)$, which describe correlated processes and is expressed in terms of the correlation function itself

$$m_q(t) = \frac{1}{2}\sum_{k,p} V(q,kp)\phi_k(t)\phi_p(t) . \tag{1b}$$

0953-8984/91/265023+23$03.50

The vertex $V(q, kp) \geqslant 0$ is given by the structure factor S_q, and is assumed to depend regularly on external control parameters. The expression in (1*b*) describes collective effects arising from cooperative motions of any particle and its surrounding. Specifically in a dense liquid this term is dominated by the so called cage effect, where any atom is to some extent trapped by the surrounding atoms for some time. This trapping mechanism introduces time dependent potential barriers, which tends to hinder local density fluctuations and thereby increases the viscosity. In the normal liquid state these barriers have a lifetime of a few collision times. When the liquid is supercooled this trapping mechanism is enhanced and may lead to a localization of a cluster of atoms for a long time. The resulting increase of the viscosity $M_q(z)$ implies a slowing down of density fluctuation, as follows from (1*a*). So there is an inherent feedback mechanism contained in these equations. When the viscosity increases density fluctuations or particle rearrangements tend to slow down. A disturbance of the atoms surrounding any other atom, will relax slower and this increases the effective barriers for particle rearrangements and thereby the viscosity and so on.

The trapping mechanism above may in an ideal case give an ergodic to non-ergodic transition at a certain temperature T_c. This is characterized by the appearence of a constant part $\phi_q(t \to \infty) = f_q$ for $T \leqslant T_c$, where f_q is referred to as the non-ergodicity parameter. A density disturbance becomes localized and does not decay with time when T becomes lower than T_c. In the ergodic liquid state for $T > T_c$, however, a density disturbance always decays and $\phi_q(t \to \infty) = 0$. In a real situation there always exist activated hopping processes, not included in (1*b*), which eventually brings the system back to the liquid equilibrium state. However, the ideal transition at T_c may still show up as a constant plateau in $\phi_q(t)$ representing a metastable state which can exist for a very long time (Das and Mazenko 1986, Das 1987, Götze and Sjögren 1987, 1988). The underlying ideal transition gives rise to a critical dynamical behaviour in $\phi_q(t)$ and other correlation functions. Close to T_c there appear two distinct slow relaxation processes, the α- and β-processes, for times t longer than a typical microscopic time t_0. The α-process describes the decay of density fluctuations on the longest time scale τ_α. The β-process exists on mesoscopic time-scales between the microscopic and α-regions. For this latter relaxation process the mode-coupling theory makes detailed and non-trivial predictions for the behaviour of $\phi_q(t)$, or any function $\phi_{XY}(qt)$, where X and Y represent variables with a non-zero overlap with the density.. Explicitly one finds (Götze 1985)

$$\phi_{XY}(qt) = f^c_{XY}(q) + h_{XY}(q)\, G(t) \tag{1c}$$

valid in the time region $t_0 \ll t \ll \tau_\alpha$. The solution in (1*c*) implies an universal behaviour since the wavevector and time dependence factorizes. The whole relaxation pattern is described by one single function $G(t)$ only.

The function $G(t)$ satisfies the equation

$$-\delta_0/z + \delta_1 G(z) + zG^2(z) + (1+\delta_2)\,\mathrm{LT}\,[G^2(t)]\,(z) + [\delta_3 + \gamma_3]\,\mathrm{LT}\,[G^3(t)]\,(z) - \gamma_3 z^2 G^3(z) + \cdots = 0 \tag{2a}$$

where the Laplace transform is defined as

$$G(z) = \mathrm{LT}\,[G(t)]\,(z) = \mathrm{i}\int_0^\infty \mathrm{d}t\, \mathrm{e}^{\mathrm{i}zt} G(t)\,. \tag{2b}$$

The parameters δ_k and γ_k can be expressed as integrals over the physical coupling constants $V(q,kp)$ in (1*b*), where the latter defines a parameter space of high dimensionality. The solution to (2*a*) show interesting properties near various bifurcation points belonging to the cuspoid family A_k. These are defined by points in the parameter space where some coefficients δ_k vanishes. Near such singular points there is a subtle low-frequency singularity in $G(z)$, which can then be classified according to the corresponding cuspoid A_k. If $\delta_0^c = \delta_1^c = 0$ but $\delta_2^c \neq 0$ we have an A_2 or Whitney fold singularity. For parameter points where also $\delta_2^c = 0$ but $\delta_3^c \neq 0$ we have an A_3 or Whitney cusp singularity and so on (Götze and Hausmann 1988, Götze and Sjögren 1989a).

Of particular importance in the present paper is the behaviour of the dielectric function $\epsilon(z)$ near the glass transition. This function can generally be expressed in terms of the electrical conductivity $\sigma(z)$ via

$$\epsilon(z) = 1 + \frac{4\pi}{z}\sigma(z) = 1 + \frac{\omega_p^2}{z}J(z). \tag{3a}$$

Here ω_p denotes the plasma frequency and $J(t) = \langle j(t)\cdot j(0)\rangle / \langle j^2(0)\rangle$, where

$$j(t) = \sum_a \sum_{i=1}^{N_a} Z_a v_{ia}(t). \tag{3b}$$

The summation in (3*b*) extends over all particles i of species a having charge numbers Z_a and velocities $v_{ia}(t)$, respectively. Since the electric current in (3*b*) is the time derivative of the total electric dipole moment, we can alternatively express $\epsilon(z)$ in terms of the dipole-dipole correlation function (Cook *et al* 1970). Introducing the memory function $M_J(t)$ of the current correlation function we find

$$\epsilon(z) = 1 - \frac{\omega_p^2}{z\,[z + M_J(z)]}. \tag{3c}$$

From this equation we can now express $\epsilon(z)$ in terms of the universal function $G(z)$ above. The memory function $M_J(z)$ can be calculated within a mode coupling approximation and is given by non-linear couplings between the partial density correlation functions. This approximation was previously derived for the special case of a two component plasma (Sjögren *et al* 1981), but is also valid in the present case. In the β-region all the partial densities behave as in (1) and so

$$M_J(z) = -f_M/z + h_M G(z) \tag{3d}$$

where f_M and h_M are expressed as wavevector integrals over coupling constants and the parameters $f_{ab}(q)$ and $h_{ab}(q)$, where a and b refers to the coupling between different components. The essential fact, however, is that, due to the factorization in (1*c*) $M_J(z)$ is given by the same function $G(z)$ as the densities. Inserting (3*d*) into (3*c*) and expanding in the small parameter $|zG(z)| \ll 1$ we find

$$\epsilon(z) = f_\epsilon + h_\epsilon z G(z) + \cdots \tag{3e}$$

where $f_\epsilon = 1 + \omega_p^2/f_M$ and $h_\epsilon = \omega_p^2 h_M / f_M^2$. Therefore, to leading order the dielectric relaxation is also ruled by the function $G(z)$. Equation (3*c*) can be used in the whole

frequency range. For lower frequencies on the liquid side $M_J(z)$ is ruled by the α-process, and satisfies a scaling behaviour $M_J(z) = M_J(z/\omega_\alpha)/\omega_\alpha$. This gives the α-relaxation scaling for $\epsilon(z)$. For sufficiently low frequencies the electrical conduction enters when free charges are present, and $\epsilon(z) = 1 + i4\pi\sigma_0/z$ with $\sigma_0 = \omega_p^2/4\pi/M_J(0)$.

The general cuspoid A_k has a canonical representation with $k-1$ relevant parameters $\delta_0, \ldots, \delta_{k-2}$. For the dynamical solution the cusp parameter $\mu_k = -\delta_k > 0$ also enter. All other parameters in (2*a*) become irrelevant for the leading order results. The Whitney fold singularity A_2 is therefore completely specified by just one separation parameter $\sigma = \delta_0$, and the exponent parameter $\lambda = 1 - \mu_2$. The function $G(t)$ is given by a conventional scaling law

$$G(t) = c_\sigma g_\pm(t/t_\sigma) . \tag{4a}$$

The solution depends, through the correlation scale c_σ and the time scale t_σ, crucially on the distance from the transition point measured via the separation parameter σ. The masterfunctions $g_\pm$ satisfy the equation (Götze 1985)

$$\mp \frac{1}{\zeta} + \zeta g_\pm^2(\zeta) + \lambda i \int_0^\infty d\tau e^{i\zeta\tau} g_\pm^2(\tau) = 0 \tag{4b}$$

where $\zeta = zt_\sigma$ and $\tau = t/t_\sigma$ are rescaled variables. Here $\pm$ refers to $\sigma \gtrless 0$, respectively. The scaling function therefore depends only on the exponent parameter λ, which is characteristic of any particular system. The solution of (4*b*) can be obtained for any value of λ (Götze 1990b). We can also obtain explicit expressions for short and long rescaled times. In the former case one finds

$$g_\pm(\tau \ll 1) = 1/\tau^a . \tag{5a}$$

For long rescaled times one finds

$$g_+(\tau \gg 1) = 1/\sqrt{1-\lambda} \tag{5b}$$

$$g_-(\tau \gg 1) = -B\tau^b \tag{5c}$$

where $B > 0$. The exponents a and b are given by the exponent parameter λ by way of

$$\lambda = \Gamma^2(1-a)/\Gamma(1-2a) = \Gamma^2(1+b)/\Gamma(1+2b) \tag{6}$$

where $0 < a < \frac{1}{2}$ and $0 < b < 1$.

The behaviour in (5*a*) implies that for short times on scale t_σ the relaxation is the same for the liquid and the glass, or non-ergodic state. This critical decay describes the motion of molecules in an almost frozen environment. For these times one cannot decide whether or not the environment is stable since the life-time of the cages is longer than t_σ. For longer times and $T < T_c$ the system arrests. For $T > T_c$ the traps break down, and this is described in the initial stage by the von Schweidler law

$$\phi_{XY}(qt) = f_{XY}^c(q) - h_{XY}(q)B(t/t'_\sigma)^b . \tag{7}$$

The new time scale t'_σ is the predicted scale for the α-relaxation process. The decay in (7) can only hold for $t/t'_\sigma \ll 1$. For larger times on scale $t'_\sigma = \tau_\alpha$ the dynamics is ruled by the α-process, which will not be considered here.

The various scales are predicted to follow algebraic variations with σ. The correlation scale in (4*a*) has a simple square root variation

$$c_\sigma = \sqrt{|\sigma|}. \tag{8a}$$

Similarly the frequency scales $\omega_\sigma = 1/t_\sigma$ and $\omega'_\sigma = 1/\tau_\alpha$ are given by

$$\omega_\sigma = 1/t_\sigma = |\sigma|^{1/2a}/t_0 \tag{8b}$$

$$\omega'_\sigma = 1/\tau_\alpha = |\sigma|^\gamma/t_0 \qquad \gamma = 1/2a + 1/2b \tag{8c}$$

Close to the transition point we can express the mathematical control parameter σ in terms of the physical control parameter $\epsilon = 1 - T/T_c$. Two kinds of behaviour appear with quite different properties (Götze 1984, Götze and Sjögren 1989a), depending on whether the non-ergodicity parameter f_q is continous or discontinous across the transition

$$\sigma \propto \epsilon^2 \qquad f^c_{XY}(q) = 0 \qquad \text{type A} \tag{9a}$$

$$\sigma \propto \epsilon \qquad f^c_{XY}(q) > 0 \qquad \text{type B}. \tag{9b}$$

Their difference can be seen clearly in the static susceptibility $\chi(q) = \chi_T(q)[1 - f(q)]$, where $\chi_T(q)$ denotes the thermodynamic susceptibility. For the type A fold we find that χ has a cusp at $T = T_c$, while for a type B fold it has a discontinuity. The former case is characteristic for a spin-glass transition (Binder and Young 1986), while the latter case appear in conventional glasses. Relation (9*a*) means that $\sigma > 0$ on both sides of the transition. Therefore for a type A fold only g_+ in (4*b*) enters, and a von Schweidler decay does not appear. For a type B fold the characteristic behaviour in (8*a*) implies a $\sqrt{|T - T_c|}$ increase of f_q for $T < T_c$. Such a behaviour has been verified quantitatively in polybutadiene by Frick *et al* (1990).

For higher order cuspoid singularities A_k the equation for $G(t)$ can also be solved, even though the solution becomes more complex (Götze and Sjögren 1989b). The general cuspoid A_k of order $k \geqslant 3$ is characterized by $\delta^c_l = 0, l = 0, \ldots, k-1$ but $\mu_k = -\delta^c_k \neq 0$. Let us introduce the transformation

$$G(t) = \rho^2 f[\ln(t/t_1)] \tag{10a}$$

where $\rho = \left[2\pi^2/3\mu_k(k-2)^2\right]^{1/2(k-2)}$ and t_1 is a microscopic time. We then obtain the differential equation for the function f (Götze and Sjögren 1989b)

$$f'^2(y) = \frac{4}{(k-2)^2} f^k(y) - g_2 f^{k-2}(y) - \cdots - g_{k-1} f(y) - g_k \tag{10b}$$

where $g_l = 4\delta_{k-l}/\mu_k(k-2)^2\rho^{2l}$ are the mathematical control parameters vanishing at the critical point. The solution to (10*b*) gives the hyperelliptic functions which satisfy the general scaling law

$$f(y; g_2, g_3, \ldots, g_k) = s^x f(sy; s^{-2x}g_2, s^{-3x}g_3, \ldots, s^{-kx}g_k) \tag{10c}$$

with $x = 2/(k-2)$. At the critical point $g_l = 0$ all l we find from (10*b*) the critical decay $f(y) = 1/y^x$ which implies

$$\phi_q(t) = f^c_q + h_q\rho^2/\ln^x(t/t_1). \tag{11}$$

Away from the critical point there are various regions in parameter space with quite different dynamics. In particular we can find the various behaviour close to the coordinate axis g_l. Here the solution describes effectively a crossover from the critical decay for $t_1 \ll t \ll t_l$ where

$$t_l = 1/\omega_l = t_1 \exp[\rho^{k-2}(|\mu_k/\delta_{k-l}|^{1/k})] . \tag{12}$$

to a new algebraic decay in $\ln(t/t_1)$ for $t \gg t_l$. Denoting the cusp temperatures collectively by T_0 we have $\delta_l \propto |T/T_0 - 1|$, and the crossover times in (12) diverges when approaching T_0 with a Vogel–Fulcher like dependence. To obtain the Laplace transform from (10*a*) we can use the general property

$$\mathrm{LT}[L(t)](z) = -(1/z)L(\mathrm{i}/z) \tag{13a}$$

that is valid asymptotically for $|z| \to 0$. Here $L(t)$ denotes a slowly varying function defined by the property $L(\alpha x)/L(t) \to 1$ for $t \to \infty$ for all $x > 0$ (Feller 1971, ch 13). From this relation we find in leading order when $|z| \to 0$

$$G(z) = -(1/z)\rho^2 f[\ln(1/-\mathrm{i}zt_1)] . \tag{13b}$$

Introducing this into (3*e*) with $z = \omega$, we can solve for the real and imaginary parts of $\epsilon(\omega)$ using the fact that $\ln(1/\omega t_1) \gg \pi/2$ for $\omega \to 0$. This gives

$$\epsilon'(\omega) = f_\epsilon - \epsilon_c f[\ln(1/\omega t_1)] , \tag{14a}$$

and

$$\epsilon''(\omega) = -\frac{\pi}{2}\epsilon_c f'[\ln(1/\omega t_1)] . \tag{14b}$$

Here $\epsilon_c = h_\epsilon \rho^2$, and $f'(y) = \mathrm{d}f(y)/\mathrm{d}y$ denotes the derivative.

For simple systems composed of spherical molecules all parameters entering in the solution can be calculated. In particular the results in (4)–(6) were succesfully compared with photon correlation measurements by van Megen and Pusey (1991) on a hard-sphere colloidal system (Götze and Sjögren 1991a). However, the results above do not depend on the detailed structure of the fluid, but only on the existence of a hidden topological singularity in the non-linear equations of motion. Also the basic physical mechanism entering the equations, with a trapping of particles in cages formed by their neighbours, must have a general validity. Therefore one may speculate that the same kind of singular dynamics appear in all liquids, irrespective of whether they are simple monatomic liquids or more complex systems like e.g. polymers. The only condition would be that one is able to come close enough to a singular point in the parameter space of the specific liquid. In particular, if experimental data on complex liquids exhibit the behaviour listed above, it supports the conclusion that the theory is of more general validity than expected from its derivation.

The purpose of the present paper is to test this hypothesis and compare the theoretical predictions with experimental data for some polymeric systems. In general the location of the singular points T_c or T_0 and the relevant frequency interval for the validity of the β-relaxation scaling laws are not known. This is due to our lack of understanding of the microscopic dynamics for complex systems like polymers, i.e. the time scales t_0 and t_1 in (8) and (10) are not known. However, we can now work backwards and test whether or not a given spectrum follows the theoretical pattern. The regular short time scales t_0 and t_1 and other parameters must in general be used as phenomenological fitting parameters. Eventually these parameters may be calculated from a microscopic theory (Schweizer 1989a,b).

2. Results

2.1. The fold

The results for the Whitney fold or A_2 singularity, are most clearly revealed in the susceptibility or the dielectric loss. The critical decay in (5*a*) implies a decrease of $\epsilon''(\omega) \propto \omega^a$ with decreasing frequency, while the von Schweidler law (5*c*) implies a subsequent increase $\epsilon''(\omega) \propto \omega^{-b}$. Hence for $T > T_c$ the β-decay process can be detected as a minimum in the dielectric loss $\epsilon''(\omega)$, which is located above the α-peak at some frequency ω_{min}. Such a minimum has been observed in polyethylene therephthalate (PET) (Ishida *et al* 1962) and analysed previously within the present scenario (Sjögren 1990a, Götze and Sjögren 1991b). A minimum in the relevant frequency region, has also been observed in polyethylene oxybenzoate PEOB (Ishida *et al* 1962), and the rescaled dielectric loss $\epsilon''(\omega)/\epsilon''_{min}$ versus ω/ω_{min}, for an amorphous sample, are shown in figure 1. Here the scaling parameter ϵ''_{min} denotes $\epsilon''(\omega_{min})$. Clearly the experimental data for different temperatures fall on a single master curve around the minimum, and the frequency interval where the data points coincide expands for decreasing temperatures. The solution to the scaling function in (4) with $\lambda = 0.80$, giving the exponents $a = 0.28$; $b = 0.48$, is also shown as a full curve. There is an overall quantitative agreement between experiments and theory, even if there is some discrepency for higher frequencies. This may indicate that the appropriate value for λ should be choosen somewhat smaller, but additional measurements for higher frequencies are necessary in order to make a more detailed comparison meaningful. Figure 1 verifies that the experimental data satisfies a scaling law, and also that the shape of the corresponding master function agrees with the predicted one.

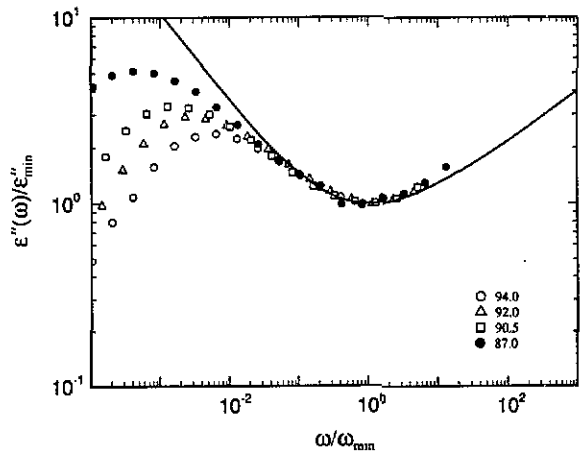

Figure 1. Rescaled dielectric loss $\epsilon''(\omega)/\epsilon''_{min}$ versus ω/ω_{min} for amorphous PEOB taken from Ishida *et al* (1962). The various symbols refer to different temperatures as indicated in the figure. Also included is the theoretical master curve obtained from (4*b*) for $\lambda = 0.80$ (full curve).

The two scales ϵ''_{min} and ω_{min} describe the variation of the minimum as the temperature changes. From (8) we find the predicted variation

$$\epsilon''_{min} \propto c_\sigma = |\sigma|^{1/2} \tag{15a}$$

$$\omega_{\min} \propto \omega_\sigma \propto |\sigma|^{1/2a} . \tag{15b}$$

From (8*c*) we also find the predicted variation of the positions of the α-peak maximum, $\omega_{\max}$

$$\omega_{\max} \propto \omega'_\sigma \propto |\sigma|^{\gamma} . \tag{15c}$$

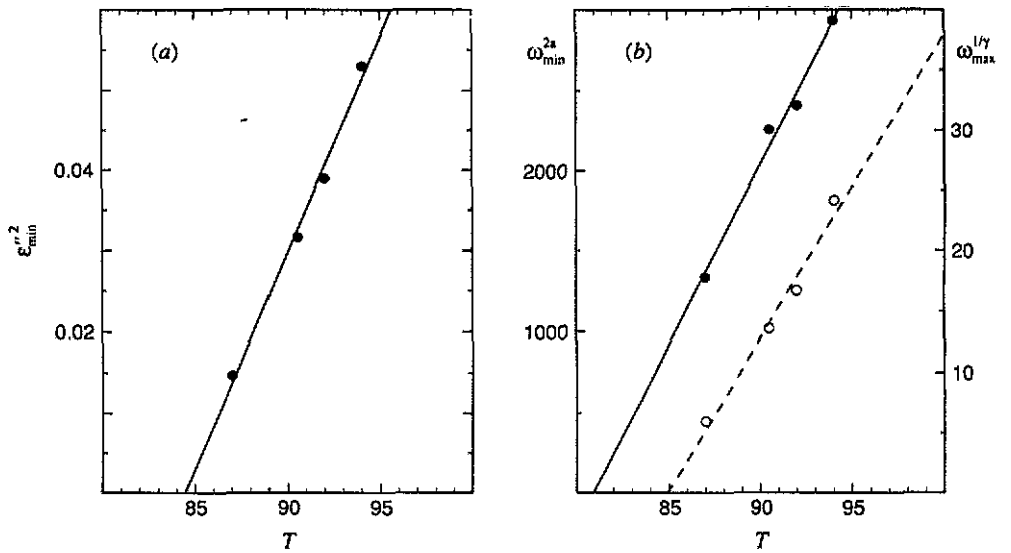

Figure 2. (*a*) Full circles, experimental values of $(\epsilon''_{\min})^2$ versus temperature T. The straight line is the best fit through the data points: it indicates the theoretical prediction in (8*a*) and (15*a*). The intersection with the abscissa gives the critical temperature T_c. (*b*) Full circles show $\omega^{2a}_{\min}$ (left scale) and open circles $\omega^{1/\gamma}_{\max}$ (right scale) versus temperature as obtained from experimental data. The full and broken straight lines are the best fits through the respective data points, and gives the theoretical predictions in (8) and (15). The intersection with the abcissa again gives the critical temperature T_c.

These results are tested in figure 2. In figure 2(*a*) we show $\epsilon''^2_{\min}$ versus temperature T. According to (15*a*) the data should fall on a straight line, which is approximately the case as shown by the full line. From the intersection with the T-axis we get an estimate of the critical temperature $T_c = 84.5$ °C. Similarly we show in figure 2(*b*) $\omega^{2a}_{\min}$ (full circles) and $\omega^{1/\gamma}_{\max}$ (open circles) versus T. The data fall again on straight lines indicated by the full and broken lines, and this supports the results in (15*b*) and (15*c*). From the intersection with the T-axis we obtain the estimates $T_c = 81$ °C and $T_c = 85$ °C, respectively. The three values of T_c agree to within a few degrees and gives the critical temperature $T_c = (83 \pm 2)$ °C. The values of the exponents $a = 0.28$ and $b = 0.48$ found above can be tested by plotting $\log \epsilon''_{\min}$ versus $\log \omega_{\min}$ and $\log \omega_{\max}$. The former plot should give a straight line with slope a and the latter a straight line with slope $ab/(a+b)$. Figure 3 shows the maxima positions (full squares) and the minima positions (full circles) for PEOB. The broken and full lines have slopes $ab/(a+b)$ and a respectively. Clearly the data are compatible with the value $a = 0.28$ and $ab/(a+b) = 0.18$. A white noise background followed by a stochastic relaxation

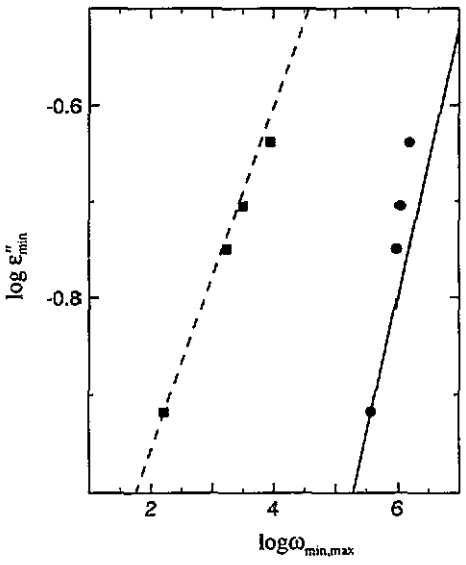

Figure 3. $\log \epsilon''_{\min}$ versus $\log \omega_{\min}$ (full circles) and $\log \omega_{\max}$ (full squares). The full and broken straight lines have slopes $a = 0.28$ and $ab/(a+b) = 0.18$, respectively.

instead of the critical spectrum and a von Schweidler law, would also result in a minimum between the high-frequency phonon peak and the α-peak. The resulting values for the exponents in that case $a = b = 1$ are clearly incompatible with the experimental data.

Together with the previously analysed PET data, the present analysis of PEOB partly verifies the theoretical results in section 1. However, for a real quantitative test of the theory we need more data at higher frequencies for both systems. Also measurements at several more temperatures are needed; in particular around the critical temperature T_c. For PEOB we find for the lowest temperature 87 °C the separation parameter $\sigma \approx -0.05$, which is still a rather large value. For PET the lowest temperature corresponds to a separation $\sigma \approx -0.03$. Measurements for temperatures below T_c but above T_g would also be of great interest. In this region hopping processes must play a significant role, and a new scaling scenario have been predicted in this case (Götze and Sjögren 1987, Sjögren 1990b). One expects also that other systems will show the characteristic behaviour found for these polymer systems, provided the relevant temperature and frequency regions are investigated.

2.2. *The cusp*

There are also experimental results on samples of PET and PEOB with various degree of crystallinity (Ishida *et al* 1962). The dielectric relaxation still originate from the amorphous part, and show the same general features as in the amorphous samples. In figure 4(*a*) we show as an example the rescaled data for PEOB with 38% degree of crystallinity, referred to as PEOB-IV by Ishida *et al* (1962), together with the theoretical master curve with $\lambda = 0.80$. For this value of the exponent parameter the theoretical curve can fit the high-frequency data, but fails for the low-frequency data. Conversely choosing a larger value of λ we can obtain better agreement for low frequencies, but will then fail for high frequencies. The corresponding values of $(\epsilon''_{\min})^2$ versus T are shown in figure 4(*b*) as full circles, and the intersection with the abscissa gives

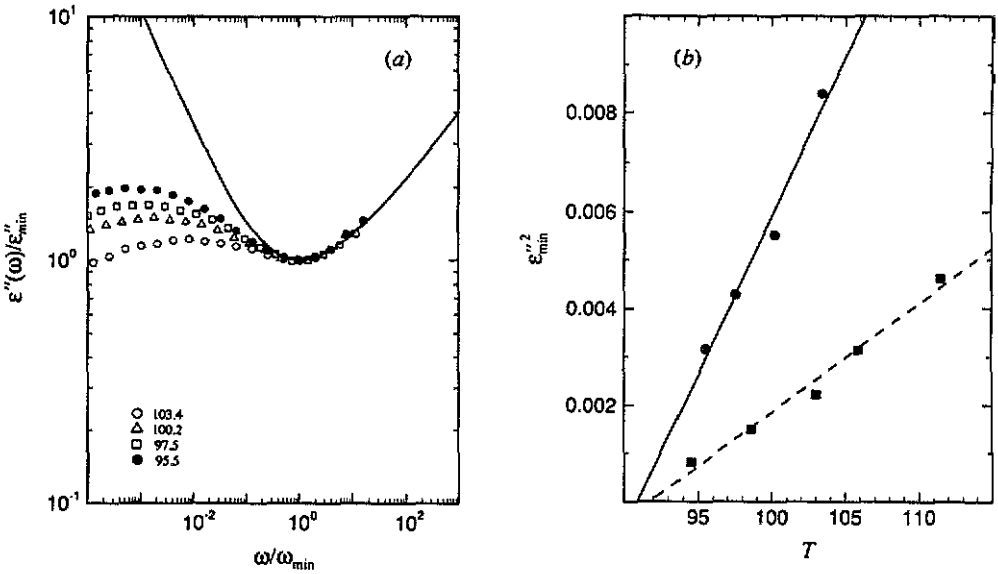

Figure 4. (*a*) Rescaled dielectric loss $\epsilon''(\omega)/\epsilon''_{min}$ versus ω/ω_{min} for PEOB with 38% degree of crystallinity taken from Ishida *et al* (1962). The various symbols refer to the different temperatures indicated in the figure. The full curve is the theoretical master curve obtained from (4*b*) for $\lambda = 0.80$. (*b*) The full circles and full squares are the experimental values of $(\epsilon''_{min})^2$ plotted versus temperature T for the samples PEOB-IV and PET-IV respectively. The full and broken straight lines are the best fit through the data points. The intersection with the abscissa gives the respective critical temperatures T_c.

the critical temperature $T_c = 91$ °C. So the data for PEOB-IV are still consistent with (15*a*), but it does not follow the predicted master curve even though the separation parameter for the lowest temperature is the same as for the amorphous sample shown in figure 1, i.e. $\sigma \approx -0.05$. Similar results are found for PET with 51% degree of crystallinity (PET-IV). The values of $(\epsilon''_{min})^2$ are also shown in figure 4(*b*) as full squares, and gives $T_c = 92$ °C. The low-frequency behaviour in figure 4(*a*) with a rather flat region indicate that these data are close to a cusp point characterised by $\lambda = 1$. Since a cusp is the meeting point of two fold lines the characteristic relaxation behaviour for such a point contain also, as a special case, that relevant for a fold with $\lambda \approx 1$. Clearly when $\lambda \to 1$ the region of validity of (5-6) decreases.

The relaxation scenario for the A_3 singularity or the cusp, is obtained from the solution of (10*b*) which gives the Weierstrass elliptic function

$$G(t) = \rho^2 \wp[\ln(t/t_1); g_2, g_3]. \tag{16}$$

valid in the time region $t_1 \ll t \ll \tau_\alpha$. Actually since the Weierstrass function is periodic, the solution may alternatively break down at the half-period where $\wp = e_1$ and e_1 is the largest real root to $4e_1^3 - g_2 e_1 - g_3 = 0$. The cusp is generically specified by two canonical separation parameters $\xi = \delta_0$ and $\eta = \delta_1$, which appear in (16) as $g_2 = 4\eta/\mu_3\rho^4$ and $g_3 = 4\xi/\mu_3\rho^6$. From (14*a*) we find for the dielectric constant

$$\epsilon'(\omega) = f_\epsilon - \epsilon_c \wp[\ln(1/\omega t_1); g_2, g_3] = f_\epsilon - c'_\xi \wp[u; \pm 12(r/4)^{1/3}, \pm 4] \tag{17a}$$

and for the dielectric loss

$$\epsilon''(\omega) = -\tfrac{1}{2}\pi\epsilon_c \wp'[\ln(1/\omega t_1); g_2, g_3] = -\tfrac{1}{2}\pi c''_\xi \wp'[u; \pm 12(r/4)^{1/3}, \pm 4] \tag{17b}$$

where

$$u = \ln(1/\omega t_1)/y_\xi \,. \tag{17c}$$

The second relations above where obtained using the scaling property in (10c) with scaling parameter $s = |\xi/\mu_3|^{1/6}/\rho$. The scales entering in (17) are predicted to have the following temperature dependence:

$$c'_\xi = h_\epsilon |\xi/\mu_3|^{1/3} \propto |T/T_0 - 1|^{1/3} \tag{18a}$$

$$c''_\xi = h_\epsilon/\rho |\xi/\mu_3|^{1/2} \propto |T/T_0 - 1|^{1/2} \tag{18b}$$

and

$$1/y_\xi = |\xi/\mu_3|^{1/6}/\rho \propto |T/T_0 - 1|^{1/6} \,. \tag{18c}$$

where T_0 denotes the location of the cusp at $\xi = \eta = 0$. To reach this point one needs in general to vary two control parameters like temperature and pressure.

The parameter r in (17) is defined as $r = |g_2^3/27g_3^2|$. The solution in (17) is therefore invariant on the lines r =const. In particular $r = 0$ and $r = \infty$ corresponds to the coordinate axis $g_2 = 0$ and $g_3 = 0$ respectively. Along these lines the Weierstrass function has relatively simple properties as well as on the line $\Delta = g_2^3 - 27g_3^2 = 0$ corresponding to $r = 1$. Here Δ denotes the discriminant and the points where $\Delta = 0$ defines the fold lines. The relevant parameter space near a cusp is shown in figure 5, where the cusp point is located at the origin. The two fold lines are given by the full and broken curves respectively. They correspond to type B folds, but the latter represent a dynamically unstable solution. The thin lines in the fourth quadrant show invariance lines where $r = 0.2$, 0.4 and 0.8. Also shown as dotted line is the case $r = \frac{1}{16}$ which appear later. Invariance curves can also be drawn in the other quadrants, but is not needed here.

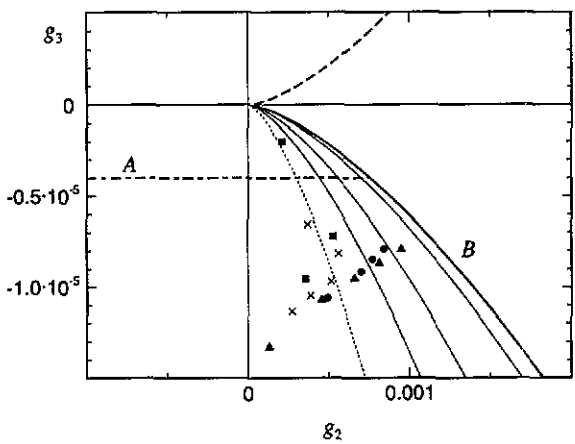

Figure 5. Relevant parameter space g_2, g_3 for a cusp singularity. The cusp point is located at the origin. The full line labelled *B* represents a type B fold, and the broken line is a corresponding unstable fold. The chain line labelled *A* represents a type A fold. The thin full curves and the dotted curve are invariance lines where $r = 0.2$, 0.4, 0.8 and 1/16 respectively. The symbols show the paths in parameter space for the various investigated systems as described in the text.

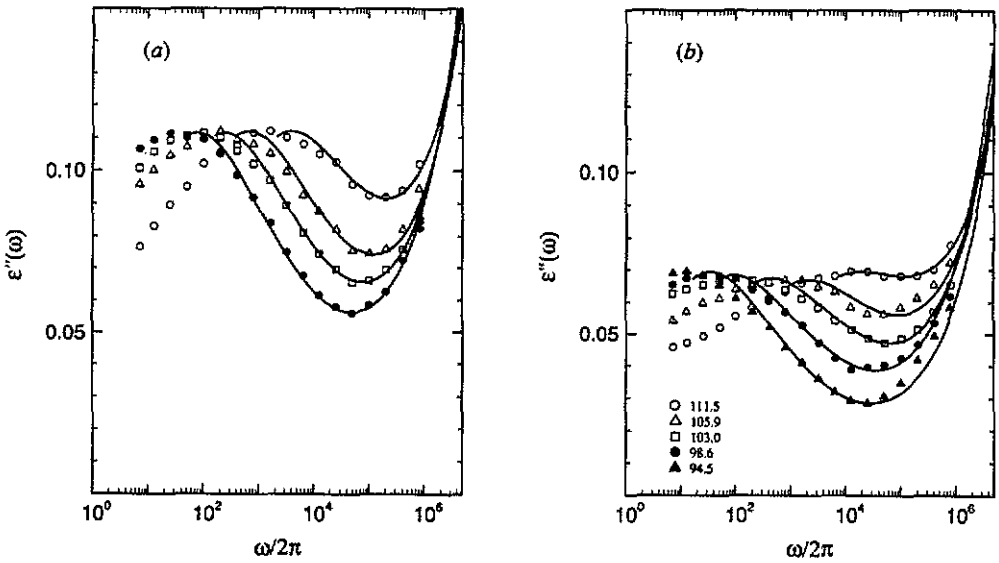

Figure 6. (*a*) $\epsilon''(\omega)$ versus ω for PEOB-IV. The various symbols correspond to those in figure 4(*a*). The full curves show the theoretical results obtained from (17*b*). (*b*) As in (*a*) but for *PET-IV*. The various symbols refer to temperatures given in the figure.

Using (17*b*) we find the dielectric loss curves shown in figure 6(*a*) and 6(*b*) for PEOB-IV and PET-IV respectively. To obtain these we must specify the four parameters ϵ_c, t_1, g_2 snd g_3. The latter two are the relevant control parameters which describe some path in parameter space when the external control parameter T is varied. These parameters can be determined approximately from the values of ϵ''_{min} and ϵ''_{max} for the respective temperatures and samples. These extreme values can be obtained from (17*b*) by differentiating and solving for the zeros of φ''. Inserting the result into (17*b*) and solving for g_2 and g_3 yields

$$g_2 = 3\left[(2/\pi^2\epsilon_c^2)((\epsilon''_{max})^2 - (\epsilon''_{min})^2)\right]^{2/3} \tag{19a}$$

and

$$g_3 = -(2/\pi^2\epsilon_c^2)((\epsilon''_{max})^2 + (\epsilon''_{min})^2)\,. \tag{19b}$$

A flat portion in ϵ'' implies therefore that $g_2 \approx 0$. The values obtained from (19) for g_2 and g_3 are shown in figure 5 for PEOB-IV (full circles) and PET-IV (full triangles).

The remaining parameters ϵ_c and t_1 can in principle be extracted from the large frequency decay. These parameters should ideally be constant, but in practice they may have some smooth temperature variation. From (17) we find the critical behaviour at large frequencies for both the real and imaginary parts

$$\epsilon'(\omega) = f_\epsilon - \epsilon_c/\left[\ln(1/\omega t_1)\right]^2 \tag{20a}$$

and

$$\epsilon''(\omega) = \pi\epsilon_c/\left[\ln(1/\omega t_1)\right]^3\,. \tag{20b}$$

In the present case there was not sufficient data at high frequencies to test this prediction, and ϵ_c and t_1 was adjusted to get an optimal fit. For PEOB-IV this gave

$\epsilon_c = 20.0$ and $1/t_1 = 25\omega^{\beta}_{max}$, where ω^{β}_{max} denotes the position of the β-peak. This was extrapolated from lower temperatures and was found to be $\log(\omega^{\beta}_{max}/2\pi) = 17.5 - 3350/T$. The corresponding values for PET-IV was $\epsilon_c = 12.0$ and $1/t_1 = 100\omega^{\beta}_{max}$ with $\log(\omega^{\beta}_{max}/2\pi) = 15.1 - 2840/T$. So ϵ_c is found to be constant, but the microscopic time t_1 has a regular Arrhenius temperature dependence. For both systems ω^{β}_{max} varies by almost a factor of two for the temperature interval considered. This regular but relevant temperature dependence of the microscopic time-scale t_1 has not yet been understood from the mode-coupling equations, and t_1 has to be used as a fitting parameter.

Clearly the results for $\epsilon''(\omega)$ obtained with these parameters agree very well with the experimental data for both systems. The solution breaks down for low frequencies $\omega \approx \omega_\alpha$ as expected, and the theoretical curves approach rapidly zero at the half period of $\wp$. The high-frequency wing of the α-peak can actually be fitted somewhat better by adjusting g_2 and g_3. For PET-IV the high-frequency points at the lowest temperature $T = 94.5$ °C, do not follow the general behaviour found for the other temperatures. For this temperature we used the value $\epsilon_c = 10$, but there are still some discrepencies. From figure 5 we see that the paths for both systems are practically the same, and approach the fold line when temperature is lowered. Since the path crosses several constant-r lines it is not possible to collapse the data onto one single master curve. For even lower temperatures the paths will cross the fold line at the respective critical temperatures T_c. Even if the paths do not approach the cusp point at the origin, this has a strong effect on the shape of the spectra. However, sufficiently close to the fold line the Weierstrass function will reduce to the previous scenario for the fold.

From figure 4(*b*) follows that the minimum ϵ''_{min} still follows a square root variation with the separation from the fold. This can be understood if we introduce the canonical coordinates σ and λ for the fold line instead of η and ξ above. The former ones can describe the relevant region $g_2 > 0$, and the transformation is given by $\eta = (1-\lambda)^3/3\mu_3$; $\xi = \sigma - \frac{2}{27}(1-\lambda)^3/\mu_3^2$ (Götze and Sjögren 1989b). Using these we find $\epsilon''_{min} = \frac{1}{2}\pi\epsilon_c\sqrt{-4\sigma/\mu_3\rho^6}$. Therefore the square root variation of the minimum, characteristic for a fold, still holds near a cusp even though the shape and position of the minimum are changed.

Another system where a cusp scenario can explain the relaxation data is polychlorotrifluoroethylene PCTFE measured by Nakajima and Saito (1958) and Scott *et al* (1962, Hoffman *et al* 1966). This is a polymer with no sidegroups capable of independent orientation, and the dielectric relaxation effects in PCTFE must therefore be attributed to motions involving portions of the chain backbone. Typical results by Scott *et al* (1962) for ϵ' and ϵ'' at $T = 118$ °, 100 ° and 75 °C are shown in figures 7(*a*) and 7(*b*). These data refer to a quenched sample with 44% crystallinity with glass transition at $T_g \approx 50$ °C (Hoffman *et al* 1966). The observed relaxation can be attributed to the amorphous liquid region. In figure 7 we have also included the theoretical results as full curves. These were obtained with $\epsilon_c = 3.5$, $1/t_1 = 20\omega^{\gamma}_{max}$, with $\log(\omega^{\gamma}_{max}/2\pi) = 16.7 - 4054/T$. Here ω^{γ}_{max} denotes the position of the main loss peak, which was attributed to the γ-process (Hoffman *et al* 1966). In the temperature interval above, ω^{γ}_{max} changes by a factor of twenty, so here t_1 cannot be treated as a constant. The values of g_2 and g_3 were obtained from (19) and are shown as full squares in figure 5.

Figure 7 shows that there is very good agreement between experiments and theory

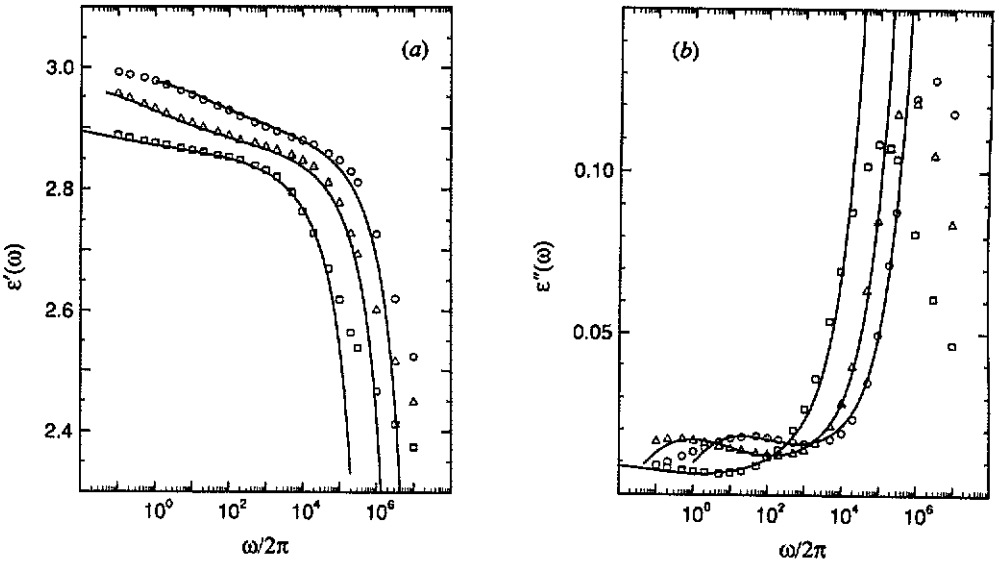

Figure 7. (*a*) $\epsilon'(\omega)$ versus ω for PCTFE at $T = 118$ °C (open circles), $T = 100$ °C (open triangles) and $T = 75$ °C (open squares) from the measurements of Scott *et al* (1962). The full curves are the theoretical results from (17*a*). (*b*) The corresponding data for $\epsilon''(\omega)$ together with the theoretical results in (17*b*) (full curves).

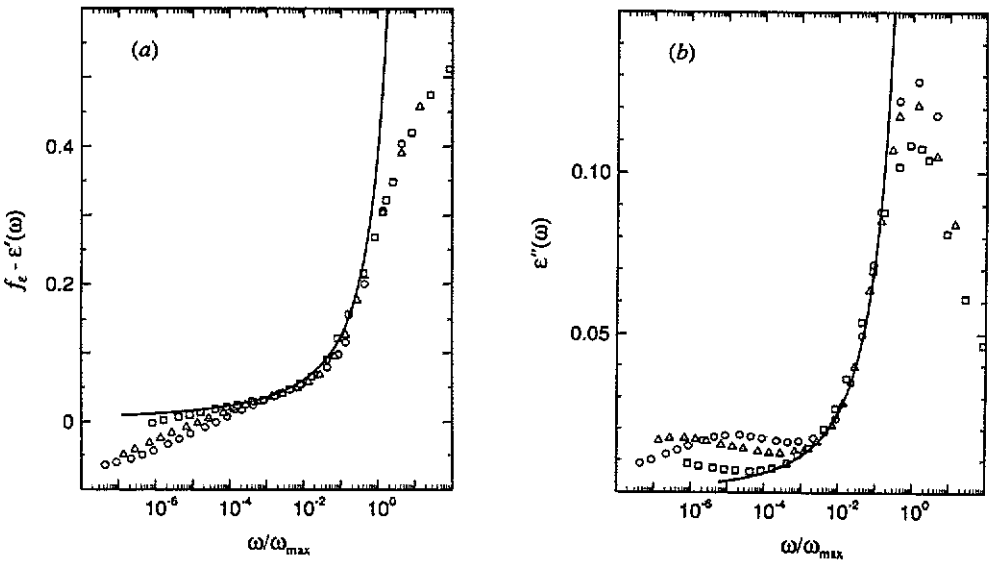

Figure 8. (*a*) $f_\epsilon - \epsilon'$ versus ω/ω_{max} for the data shown in figure 7(*a*), and with the same symbols. The full curve represent the critical decay in (20*a*) with $\epsilon_c = 3.5$ and $1/t_1\omega_{max} = 20$. (*b*) $\epsilon''(\omega)$ versus ω/ω_{max} for the same data as in figure 7(*b*). The full curve show the predicted behaviour in (20*b*) with the same parameters as in (*a*). Here ω_{max} denotes the position of the main loss maximum in ϵ''.

in a frequency interval extending four to six decades below the main peak. The parameters ϵ_c and t_1 could in this case be extracted from the high-frequency behaviour where (20) must hold. Except for the regular variation of the parameters (20) implies a temperature independent shape of the spectra. It is an essential test of the theory that the data of Scott *et al* satisfy this property. This is verified in figure 8(*a*) and 8(*b*) where we show $f_\epsilon - \epsilon'(\omega)$ versus $\omega/\omega_{max}^{\gamma}$ and $\epsilon''(\omega)$ versus $\omega/\omega_{max}^{\gamma}$ respectively, together with the theoretical prediction in (20) (full curves). Clearly all data points fall on temperature independent master curves in a rescaled frequency interval of more than one decade below the peak, and the shape is very well given by (20) with parameters $\epsilon_c = 3.5$ and $1/t_1\omega_{max}^{\gamma} = 20$. The data are therefore compatible with a temperature independent critical spectrum provided one allows for a relevant Arrhenius temperature dependence for the microscopic time t_1. For the lowest temperature $T = 75$ °C the data follow the critical behaviour for three to four decades, so this point is rather close to the cusp as is also seen in figure 5. The parameter f_ϵ has a smooth almost linear temperature dependence, and is shown in figure 11 later.

The full squares in figure 5 are close to the line $g_2 = 0$. In this case the low-frequency behaviour of (17) can be found explicitly. Along this axis there is a crossover from the critical behaviour in (20) for frequencies $1/t_1 \gg \omega \gg \omega_\xi$, where $\omega_\xi = \omega_3$ in (12), to the low-frequency behaviour

$$\epsilon'(\omega) = f_\epsilon - 3c'_\xi + 2c''_\xi \ln(1/\omega t_1) \tag{21a}$$

and

$$\epsilon''(\omega) = \pi c''_\xi \tag{21b}$$

valid for $\omega \ll \omega_\xi$. *A characteristic property of a cusp, in the parameter region* $g_2 \approx 0$, is therefore a linear increase as $\ln\omega$ with decreasing ω for the real part, and a constant frequency independent behaviour for the imaginary part at low frequencies. These general features are seen in figure 7

The path in parameter space followed by PCTFE is clearly different compared with the previous ones. From figure 5 we see that the full squares approach the origin when temperature is lowered, and follow approximately the dotted curve corresponding to the value $r = \frac{1}{16}$. Therefore the shape of the spectra should show more cusp like features than those in figure 6, and also be almost invariant for different temperatures. This implies that it must be possible to rescale the data for the various temperatures so that they fall on one single master function. Also the scales should have the temperature dependence in (18). Such scaling plots of the data of Scott *et al* are shown in figures 9(*a*) and 9(*b*) for ϵ' and ϵ'' respectively. In the frequency region $\omega < \omega_{max}^{\gamma}$ all data falls on master curves, and the region where the points coincide expands when temperature is lowered. The full curves show the predicted master functions given by $\wp[u; 3, -4]$ and $-\frac{1}{2}\wp'[u; 3, -4]$ respectively corresponding to the value $r = \frac{1}{16}$. The small scattering of the data points around the full curves arises because the path in parameter space do not exactly follow an invariance line r =const when temperature is varied. The small deviation from a straight line for large values of u in figure 9(*a*) and the small fluctuations around a constant in figure 9(*b*) in both the data points and theoretical curves arises because we are slightly away from the line $g_2 = 0$. Increasing the value of r towards $r = 1$ will enhance these effects as shown in figure 6. The low-frequency peaks in figure 6 clearly reflects the α-relaxation process and are characteristic for the behaviour near a fold-line. From figures 7 and 9 we conclude that the low frequency loss peaks are described rather well by the

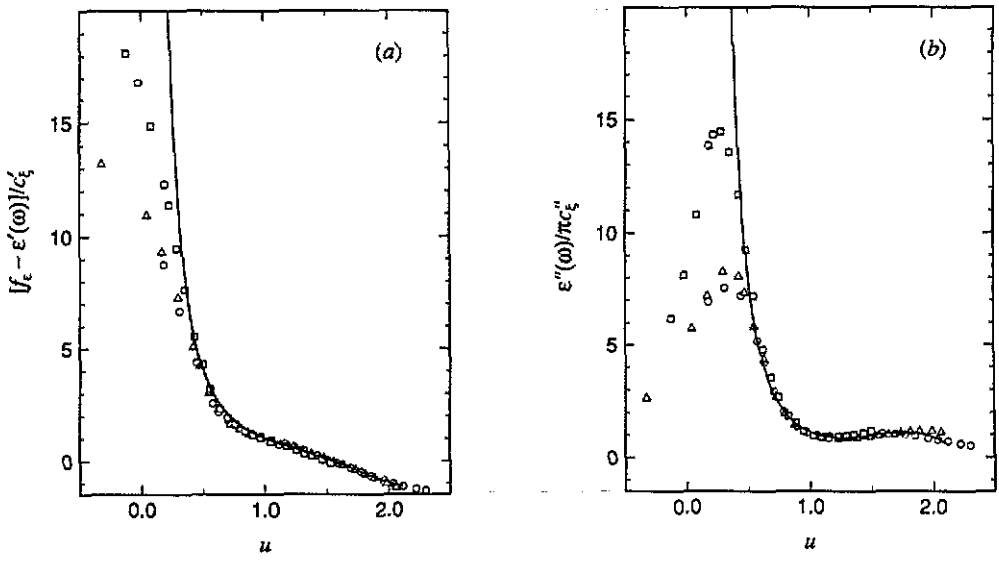

Figure 9. (*a*) Rescaled dielectric constant $[f_\epsilon - \epsilon'(\omega)]/c'_\xi$ versus $u = \ln(1/\omega t_1)/y_\xi$ with symbols as in figure 7. The full curve is the predicted master curve $\wp[u; 3, -4]$ in (17*a*). (*b*) Rescaled dielectric loss $\epsilon''(\omega)/\pi c''_\xi$ versus u for the data in figure 7(*b*). The full curve is the predicted master function $-\frac{1}{2}\wp'[u; 3, -4]$ in (17*b*). The theoretical curves are cut off slightly below the half-period of $\wp$.

β-relaxation function, which was not the case for the previous systems in figure 6. Therefore in this case the low-frequency peak should rather be treated as a part of the β-process (Hoffman *et al* 1966), and reflects the dynamics of the $g_2 = 0$ line rather than the fold line in figure 5.

The parameters used in the scaling plots above are shown in figures 10 and 11 below. The parameters c'_ξ and y_ξ used to rescale the real part are shown as open squares in figure 10. These were extracted in the following way. From (21*a*) we see that the slope of the linear part in ϵ' for low ω is given by $2c''_\xi$. This slope could be determined for the various temperatures, and the resulting values of c''_ξ are shown as crosses in figure 11a. From this value of c''_ξ and the value of the critical amplitude ϵ_c above, we can determine c'_ξ and y_ξ since from (18)

$$c''_\xi = c'_\xi / y_\xi \tag{22a}$$

and

$$c'_\xi y_\xi^2 = \epsilon_c. \tag{22b}$$

The last relation implies that $y_\xi = \ln(1/\omega_\xi t_1)$ is determined from the frequency where the two asymptotic results in (20*a*) and (21*a*) intersect. Similarly from the almost straight line part in figure 7(*a*) we can determine the regular constant f_ϵ using (21*a*) and the previous values of c'_ξ, y_ξ and t_1. The resulting values are shown in figure 11, and was used before to obtain figure 8(*a*). The parameters c''_ξ and y_ξ used to rescale the imaginary part were extracted independently from ϵ'' and are shown as open circles in figure 10. The values of c''_ξ was extracted from the average value of the plateau in $\epsilon''(\omega)$ for low frequencies. From these values we determine corresponding values of y_ξ from the intersection of this plateau with the critical spectrum or from

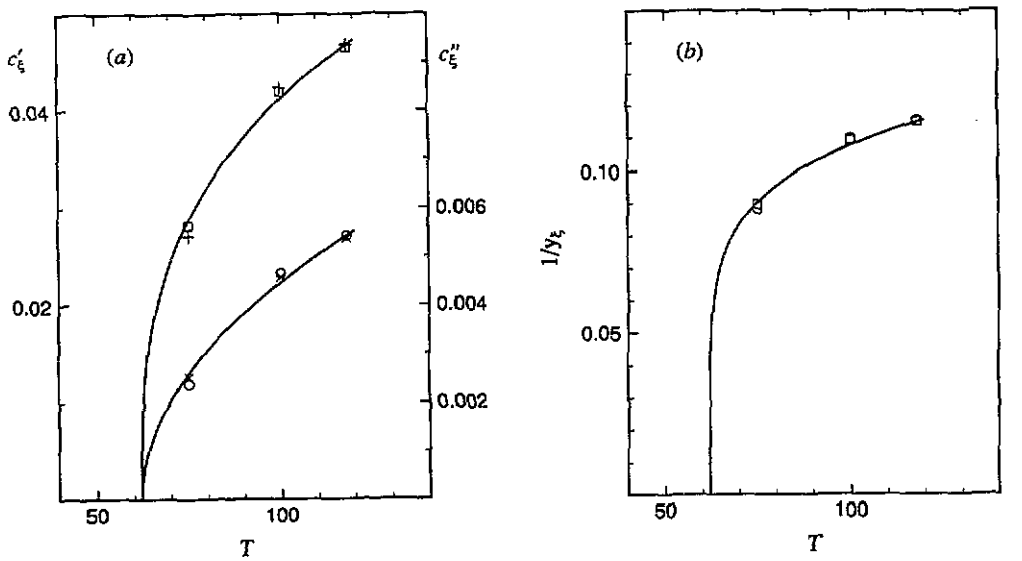

Figure 10. Scaling parameters c'_ξ (open squares) and c''_ξ (open circles) extracted from ϵ' and ϵ'' respectively. These parameters were used to obtain the scaling plots in figure 9. The crosses show the values of c''_ξ extracted from the slope in ϵ' and the plus signs the values of c'_ξ extracted from ϵ''. The full curves show the predicted behaviour $c'_\xi \propto |T/T_0 - 1|^{1/3}$ and $c''_\xi \propto |T/T_0 - 1|^{1/2}$ with $T_0 = 62$ °C. (*b*) The scaling parameter $1/y_\xi$ obtained from ϵ' (open squares) and ϵ'' (open circles) respectively. The full curve show the predicted behaviour $1/y_\xi \propto |T/T_0 - 1|^{1/6}$ with $T_0 = 62$ °C as in (*a*).

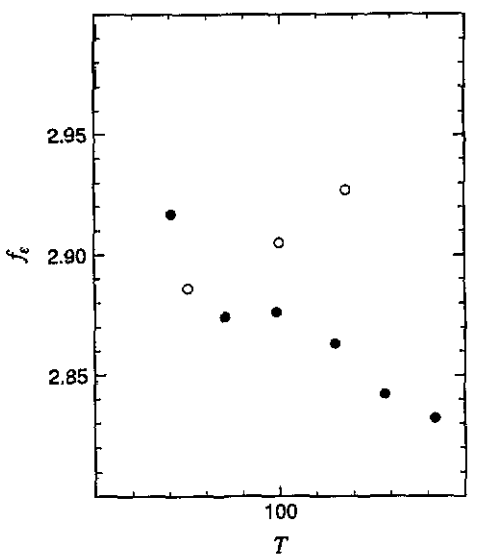

Figure 11. The values of f_c used in the rescaling of ϵ' in figures (8*a*), (9*a*) and (12*a*). The open circles refer to the data of Scott *et al* (1962), and the full circles to those of Nakajima and Saito (1958).

(22) $c''_\xi y_\xi^3 = \epsilon_c$. With the values of c''_ξ and y_ξ obtained in this way from ϵ'' we can also determine a second set of values for c'_ξ using (22*a*). These are shown as plus signs

in figure 10(*a*). Clearly the two sets of scaling parameters extracted independently from ϵ' and ϵ'' are identical, as they should be. We can now compare these data with the theoretical predictions in (18). Plots of the parameters c'_ξ, c''_ξ and $1/y_\xi$ raised to the exponents 3, 2 and 6 respectively gave, with the reservation for the limited number of points, straight lines wich intersected the T-axis at a common temperature $T_0 = (62 \pm 4)$ °C. So the data are consistent with a cusp at a temperature T_0 twelve degrees above the calorimetric glass temperature T_g. The predicted variation of the scaling parameters obtained from the straight lines are shown as full curves in figure 10. Clearly more data points in the region around T_0 are necessary in order to verify or disprove the predicted functional forms. There also exist data for lower temperatures $T < T_0$ (Scott *et al* 1962). These were also consistent with the critical spectra in (20) with the same value of t_1 but with a value $\epsilon_c \approx 5$. So there is an asymmetry in the data not predicted by the mode coupling theory. Similar results were found in orientational glasses by Michel (1987), and there this problem was resolved by allowing for a change in the coupling constants when the static response changes. No scaling plots could be obtained for $T < T_0$ since the low-frequency data ran out of the experimental window. Therefore experimental data for lower frequencies are necessary in this case.

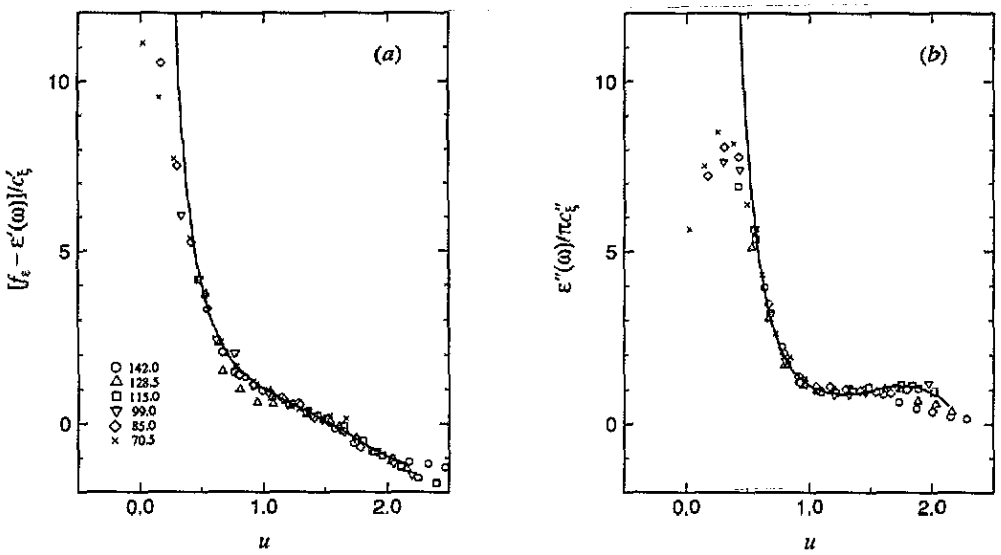

Figure 12. (*a*) Rescaled dielectric constant $[f_\epsilon - \epsilon'(\omega)]/c'_\xi$ versus $u = \ln(1/\omega t_1)/y_\xi$ From the data of Nakajima and Saito (1958) for the various temperatures indicated in the figure. The full curve is the predicted master curve $\varphi[u; 3, -4]$ in (17*a*). (*b*) Rescaled dielectric loss $\epsilon''(\omega)/\pi c''_\xi$ versus u for the same data as in (*a*). The full curve is the predicted master function $-\frac{1}{2}\varphi'[u; 3, -4]$ in (17*b*)

More extensive data for PCTFE was obtained by Nakajima and Saito (1958) for an annealed sample slowly cooled from the melting point. The degree of crystallinity at 23 °C was 49%. The annealed sample have a much lower glass transition temperature $T_g < -80$ °C (Hoffman 1952) than that considered above. However, for all the available temperatures $T \geqslant 70$ °C, where scaling parameters could be extracted, the data were compatible with a critical spectrum with the same parameters as for the

quenched case, i.e. $\epsilon_c = 3.5$ and $1/t_1 = 20\omega_{max}^{\gamma}$, with $\log(\omega_{max}^{\gamma}/2\pi) = 17.7 - 4409/T$. The path in parameter space for this sample is shown by the crosses in figure 5. For the lowest temperature considered, $T = 70.5$ °, it was not possible to extract values of g_2 and g_3. Again this path follows approximately the invariance line $r = \frac{1}{16}$, although there is more scattering in the points for this case. The rescaled data are shown in figure 12(*a*) and 12(*b*) together with the theoretical curves $\wp[u;3,-4]$ and $-\frac{1}{2}\wp'[u;3,-4]$. The scaling parameters used in these plots are given in figures 13 and 11, with the same symbols as used in figure 10. The data are consistent with a singular point at $T_0 = (19 \pm 5)$ °C and the overall temperature dependencies are consistent with that in (18). However, in this case the data show more scattering, and the two sets of parameters extracted independently from ϵ' and ϵ'' do not agree perfectly as in the previous case.

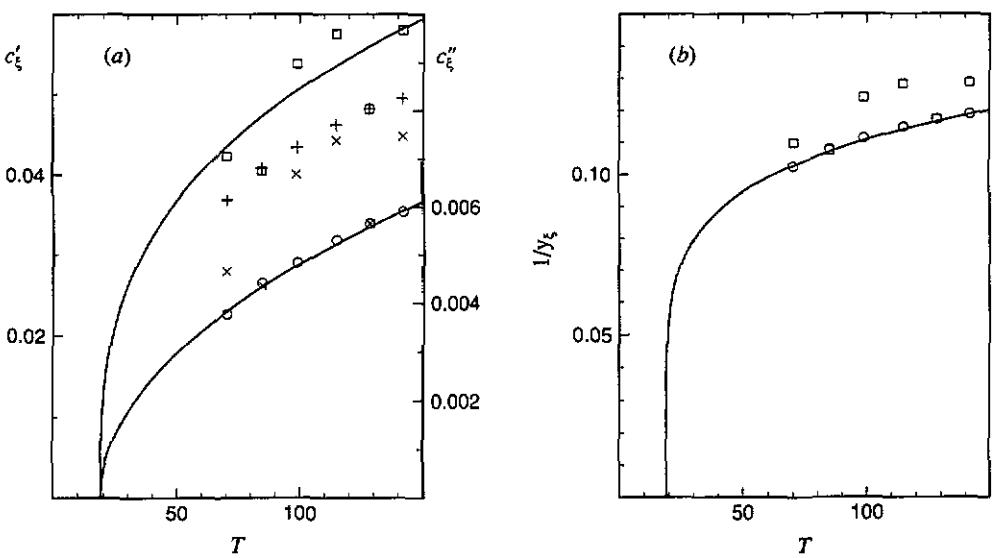

Figure 13. Scaling parameters c_ξ' and c_ξ'' corresponding to the scaling plots in figure 12, and with symbols as in figure 10(*a*). The full curves show the predicted behaviour $c_\xi' \propto |T/T_0 - 1|^{1/3}$ and $c_\xi'' \propto |T/T_0 - 1|^{1/2}$ with $T_0 = 19$ °C. (*b*) The corresponding values of $1/y_\xi$ as in figure 10(*b*). The full curve show the predicted behaviour $1/y_\xi \propto |T/T_0 - 1|^{1/6}$ with $T_0 = 19$ °C as in (*a*).

The broken fold line in figure 5 corresponds to an unphysical solution, and the cusp appears therefore as an endpoint to the full fold line at the temperature T_0. Such an endpoint must lie below a second fold line indicated by the chain curve in figure 5, otherwise is would be possible to come from a non-ergodic state to an ergodic one without passing a transition point (Götze and Hausmann 1988). The location of this fold line, with respect to the cusp, will vary from system to system, and in figure 5 it refers to the data of Nakajima and Saito (1958). This second fold may be of type A or type B. Therefore before we come close to a cusp located at $T = T_0$ we pass a fold singularity at a higher temperature $T = T_c$. Depending on the path in parameter space the competing singularities may affect different frequency regions. In the present case there is no sign of a von Schweidler increase of the spectrum

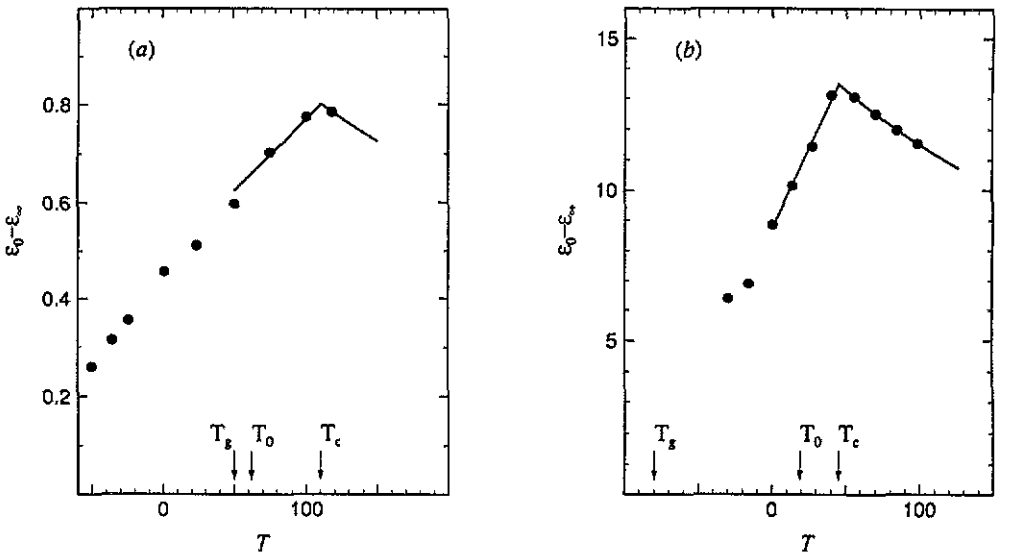

Figure 14. (*a*) Static susceptibility $\epsilon_0 - \epsilon_\infty$ versus temperature for the data of Scott *et al* (1962). The cusp is located at $T_c = 110$ °C. The full curve for $T > T_c$ show a $1/T$ law and that for $T < T_c$ a straight line. These curves indicate the theoretical predictions for a type A fold. The arrows indicate also the location of the cusp temperature $T_0 = (62 \pm 4)$ °C and the calorimetric glass transition temperature $T_g = 50$ °C. (*b*) As in (*a*) for the data of Nakajima and Saito (1958). Here the vertical axis have been multiplied by a factor 1000. The arrows indicate the critical temperature $T_c = 45$ °C, $T_0 = 19$ °C and $T_g \leqslant -80$ °C.

for low frequencies, and this indicates that the chain curve represents a type A fold. This conclusion follows also from direct physical arguments. The samples contain a crystalline component which essentially does not affect the relaxation spectra. For the 40–50% degree of crystallization these regions are relatively small in size and disorganized with respect to their mutual orientation. They will therefore act as static scattering centers for the relaxation of polar groups in the amourphous regions. The appearence of static scattering centers has been treated in various contexts (Götze *et al* 1981a,b, Götze and Sjögren 1984, Michel 1987), and is known to give a cusp in the static susceptibility as is typical for a type A fold. In the present case the static susceptibility is given by

$$\epsilon_0 - \epsilon_\infty = \frac{2}{\pi} \int_0^\infty \mathrm{d}(\ln \omega)\, \epsilon''(\omega)\,. \tag{23}$$

The temperature dependence of $\epsilon_0 - \epsilon_\infty$ for the two sets of data for PCTFE are shown in figure 14. Clearly there is a sharp cusp at $T = T_c = 45$ °C in the data of Nakajima and Saito (1958) shown in figure 14(*b*), while there is an indication of a cusp at $T = T_c = 110$ °C in the data of Scott *et al* shown in figure 14(*a*). Subtracting some contribution in $\epsilon_0 - \epsilon_\infty$ from the crystalline region tends to give a more pronounced cusp (Scott *et al* 1962, figure 23(*a*)). In figure 5 the chain line labelled *A* illustrates the situation for the data of Nakajima and Saito (1958). Lowering the temperature the path will eventually cross this line while approaching the cusp. For the data of Scott *et al* (1962) a corresponding fold line at $T = 110$ °C can be drawn between the

two most distant squares. In this case $T = 75$ °C lies below this line. The finding of a cusp in the static susceptibiulity at a temperature $T_c > T_0$ is a strong support for the theory. In the dynamical dielectric data the presence of this additional singularity could show up as an algebraic tail for very low frequencies.

3. Discussion

The results above show that the relaxation scenarios predicted by the mode-coupling theory of supercooled liquids, can be found in real systems. Together with the previously analysed PET data (Sjögren 1990a) and the light scattering data on hard-sphere colloidal systems (Götze and Sjögren 1991a), one may conclude that there is a quantitative agreement between theory and experimental results. This may also be concluded from neutron scattering measurements on a variety of systems (see Richter *et al* 1989).

The mode coupling theory was originally formulated for simple one component systems with spherical symmetric interactions. It may therefore be argued that it cannot be applied to such complex systems as polymers. However, the results obtained reflect a bifurcation scenario in the non-linear equations (Ioss and Jacobs 1980), which may exist in all liquids independent of complexity. The shape of the relaxation spectra in the β-region described by the function $G(z)$ is ruled by a few relevant parameters characterising a topological singularity. Therefore anticipating the dynamical behaviour in section 1, we can work backwards and look for systems where such relaxations seems to appear. Obviously the results above indicate that the A_2 and A_3 cases are realised in some polymers.

The master functions $g_\pm$ for the fold are not completely universal, but depend on one single number, namely the exponent parameter λ. This depends on the structural details entering through the physical coupling constants $V(q, kp)$, and will therefore vary from system to system. Systems with the same value of λ will have the same scaling functions $g_\pm$. In general for more complex systems λ cannot be calculated since the static structure is not known well enough. In data analysis we have in practice to treat λ as a fitting parameter as was done here for *PEOB* and earlier for PET. So far λ and other parameters in the theory have only been calculated for simple hard shere (Bengtzelius *et al* 1984, Barrat *et al* 1989) and Lennard-Jones (Bengtzelius 1986a,b) systems. For the former system quantitative agreement without any adjustable parameters was obtained with light scattering measurements on a colloidal system (Götze and Sjögren 1991a).

For the higher order cuspoids A_k; $k \geqslant 3$ there is complete universality regarding the shape of the relaxation function. For the cusp A_3 for instance, we find the Weierstrass function $\wp$ as the relevant master function independent of the particular system studied. Various systems differ only with respect to the cusp parameter μ_k, which enter the amplitude ρ and the various separation or scaling parameters g_l. In practice, however, we do not know the precise path followed by a particular system in parameter space $g_2, \ldots, g_k$, when varying a relevant control parameter like temperature. Therefore one or more of the parameter g_l may have to be treated as fitting parameters in analysing a particular experiment. For the special case of the cusp there are only two relevant control parameters and we can write

$$\begin{pmatrix} g_2 \\ g_3 \end{pmatrix} = \begin{pmatrix} A_{11} & A_{12} \\ A_{21} & A_{22} \end{pmatrix} \begin{pmatrix} T - T_0 \\ X - X_0 \end{pmatrix} \tag{24}$$

where X denotes some variable, like pressure or degree of crystallinity, in addition to temperature. Therefore by determining the matrix elements A_{kl} and the cusp point T_0, X_0 we can find the relation between the physical control parameters T, X and the mathematical ones g_2, g_3. By a suitable choice of the former ones one can in principle map out the complete region around a cusp singularity and possibly verify whether the Weierstrass function gives the correct behaviour or not. In particular it would be highly interesting to precisely follow various r =const. lines, where φ has simple scaling properties. These properties are quite different in various sectors of the $g_2 - g_3$ plane. (Götze and Sjögren 1989b, Götze 1989).

The relaxation functions can also be studied directly in timespace, where comparison can be made with photon-correlation or neutron spin-echo spectroscopy. Considering the cusp we predict the behaviour in (16) for the relaxation function. For short times this gives the critical spectrum in (11) with $x = 2$, while the long time behaviour corresponding to the low frequency behaviour in figure 7 gives a $-\ln(t/t_1)$ decay. Together with the cusp in the static susceptibility shown in figure 14 this is similar to what is found in spin-glasses. It was previously suggested that the spin-glass transition is related to an A_3 cusp below a type A fold (Götze and Haussmann 1988, Götze and Sjögren 1984, 1989b).

Acknowledgments

The author is greatful to Professors W Götze and A Sjölander for useful discussions and for comments on the manuscript. This work was supported by the Swedish Natural Science Research Council.

References

Barrat J L, Götze W and Latz A 1989 *J. Phys.: Condens. Matter* **1** 7163
Bengtzelius U 1986a *Phys. Rev.* A **33** 3433
—— 1986b *Phys. Rev.* A **34** 5059
Bengtzelius U, Götze W and Sjölander A 1984 *J. Phys. C: Solid State Phys.* **17** 5915
Binder K and Young A P 1986 *Rev. Mod. Phys.* **58** 811
Cook M, Watts D C and Williams G 1970 *Trans. Faraday Soc.* **66** 2503
Das S P 1987 *Phys. Rev.* A **36** 211
Das S P and Mazenko G F 1986 *Phys. Rev.* A **34** 2265
Feller W 1971 *An Introduction to Probability Theory and its Applications* vol 2, 2nd edn (New York: Wiley)
Frick B, Farago B and Richter D 1990 *Phys. Rev. Lett.* **64** 2921
Götze W 1984 *Z. Phys.* B **56** 139
—— 1985 *Z. Phys.* B **60** 195
—— 1987 *Amorphous and Liquid Materials* ed E Lüscher, G Fritsch and G Jacucci (Dordrecht: Martinus Nijhoff) p 34
—— 1989 *Proc. 5th International Symposium on Selected Topics in Statistical Mechanics* (Singapore: World Scientific) p 110
—— 1990a *Liquids, Freezing and the Glass Transition* ed D Lesvesque, J-P Hansen and J Zinn-Justin (Amsterdam: Elsevier)
—— 1990b *J. Phys.: Condens. Matter* **2** 8485
Götze W and Haussmann R 1988 *Z. Phys.* B **72** 403
Götze W, Leutheusser E and Yip S 1981 *Phys. Rev.* A **23** 2634
—— 1981b *Phys. Rev.* A **24** 1008
Götze W and Sjögren L 1984 *J. Phys. C: Solid State Phys.* **17** 5759
—— 1987 *Z. Phys.* B **65** 415

—— 1988 *J. Phys. C: Solid State Phys.* **21** 3407
—— 1989a *J. Phys.: Condens. Matter* **1** 4183
—— 1989b *J. Phys.: Condens. Matter* **1** 4203
—— 1991a *Phys. Rev.* A at press
—— 1991b *J. Non-Cryst. Solids* at press
Hoffman J D 1952 *J. Am. Chem. Soc.* **74** 1696
Hoffman J D, Williams G and Passaglia E 1966 *J. Polym. Sci.* C **14** 173
Ioos G and Joseph D D 1980 *Elementary Stability and Bifurcation Theory* (Berlin: Springer)
Ishida Y, Yamafuji K, Ito H and Takayanagi M 1962 *Koll. Z. Z. Polym.* **184** 97
Nakajima T and Saito S 1958 *J. Polym. Sci.* **31** 423
Michel K H 1987 *Z. Phys.* B **68** 259
Pusey P N and van Megen W 1987 *Phys. Rev. Lett.* **59** 2083
—— 1990 *Ber. Bunsenges. Phys. Chem.* **94** 225
Richter D, Dianoux A J, Petry W and Teixeira J 1989 *Dynamics of Disordered Materials* (Berlin: Springer)
Schweizer K S 1989a *J. Chem. Phys.* **91** 5802
—— 1989b *J. Chem. Phys.* **91** 5822
Scott A H, Scheiber D J, Curtis A J, Lauritzen J I and Hoffman J D 1962 *J. Res. Natl Bur. Stand* A **66** 269
Sjögren L 1990a *Basic Features of the Glassy State* eds Colmenero J and Alegria A (Singapore: World Scientific) p 137
—— 1990b *Z. Phys.* B **79** 5
Sjögren L, Hansen J P and Pollock E L 1981 *Phys. Rev.* A **24** 1544
van Megen W and Pusey P N 1991 *Phys. Rev.* A at press